EUROPEAN ORGANIZATION FOR NUCLEAR RESEARCH

CERN/PS 92-45 (AR)

ELECTRON BEAM COOLING AND BEAM INSTABILITY STUDIES AT LEAR

J. Bosser, M. Chanel, R. Ley, D. Möhl, U. Oeftiger, G. Tranquille

ABSTRACT

The electron cooling device installed on LEAR is now an integral part of the machine and is used to improve the beam quality and the machine duty cycle at momenta lower than 309 MeV/c. In this paper we will briefly describe the LEAR machine and the cooler and then present the results of cooling experiments performed on a variety of ion beams. The problem of instabilities in machines using electron cooling devices will also be presented and finally we will discuss the future of electron cooling at LEAR.

Paper presented at the International Workshop on Physical Experiments and First Results on Heavy ion Storage and Cooler Rings, Smolenice, June 1st-5th, 1992.

Geneva, Switzerland
August 1992

ELECTRON BEAM COOLING AND BEAM INSTABILITY STUDIES AT LEAR

J. Bosser, M. Chanel, R. Ley, D. Möhl, U. Oeftiger, and G. Tranquille
PS Division, CERN, CH-1211 Geneva 23

ABSTRACT

The electron cooling device installed on LEAR is now an integral part of the machine and is used to improve the beam quality and the machine duty cycle at momenta lower than 309 MeV/c. In this paper we will briefly describe the LEAR machine and the cooler and then present the results of cooling experiments performed on a variety of ion beams. The problem of instabilities in machines using electron cooling devices will also be presented and finally we will discuss the future of electron cooling at LEAR.

1. INTRODUCTION

Electron cooling has proved to be an invaluable tool for obtaining high-quality beams of ions at ultra-low momenta. Its full integration in the LEAR machine has necessitated a number of major upgrades on the original design [1] and has enabled us to fully investigate the problems of instabilities with strongly cooled beams. Moreover, a considerable number of physics experiments at LEAR greatly benefit from the use of electron cooling which reduces cooling times for deceleration to the utmost minimum.

2. THE LEAR MACHINE

The Low Energy Antiproton Ring (LEAR) at CERN [1] is a 78 m storage/stretcher ring designed to deliver beams of extremely high quality to physics experiments in the momentum range between 2 GeV/c and 61.2 MeV/c (Fig. 1). The essential features of the machine are phase-space cooling for improving the beam quality and ultra-slow stochastic extraction with spill times ranging from 0.5 hour to 3 hours. Fast extraction is also possible at low momenta for experiments using Penning traps for precision mass measurements or for further deceleration in an inverse radio-frequency quadrupole linac (RFQ). In addition to the extracted beams, an internal gas jet target has also been installed in the machine working at momenta above 609 MeV/c [2].

A typical LEAR cycle (Fig. 2) will involve the transfer of a batch of about 5×10^9 antiprotons from the Antiproton Accumulator (AA) which are then decelerated in the Proton Synchrotron (PS) from 3.5 GeV/c to 609 MeV/c and then injected into LEAR. At injection the beam is cooled using stochastic cooling for about 5 minutes before being either accelerated or decelerated to the required momentum for physics. On the deceleration cycle the beam is held on a series of fixed momentum 'flat-tops' (309, 200, 105, and 61.2 MeV/c) for intermediate cooling. At these momenta electron cooling is usually used in the 'pulsed mode' as it greatly improves the duty cycle; this will be explained in chapter 3. During the ultra-slow extraction process stochastic cooling is applied in order to maintain beam quality during the long extraction, except at 61.2 MeV/c where only electron cooling is possible. Table 1 gives the main characteristics of the LEAR machine.

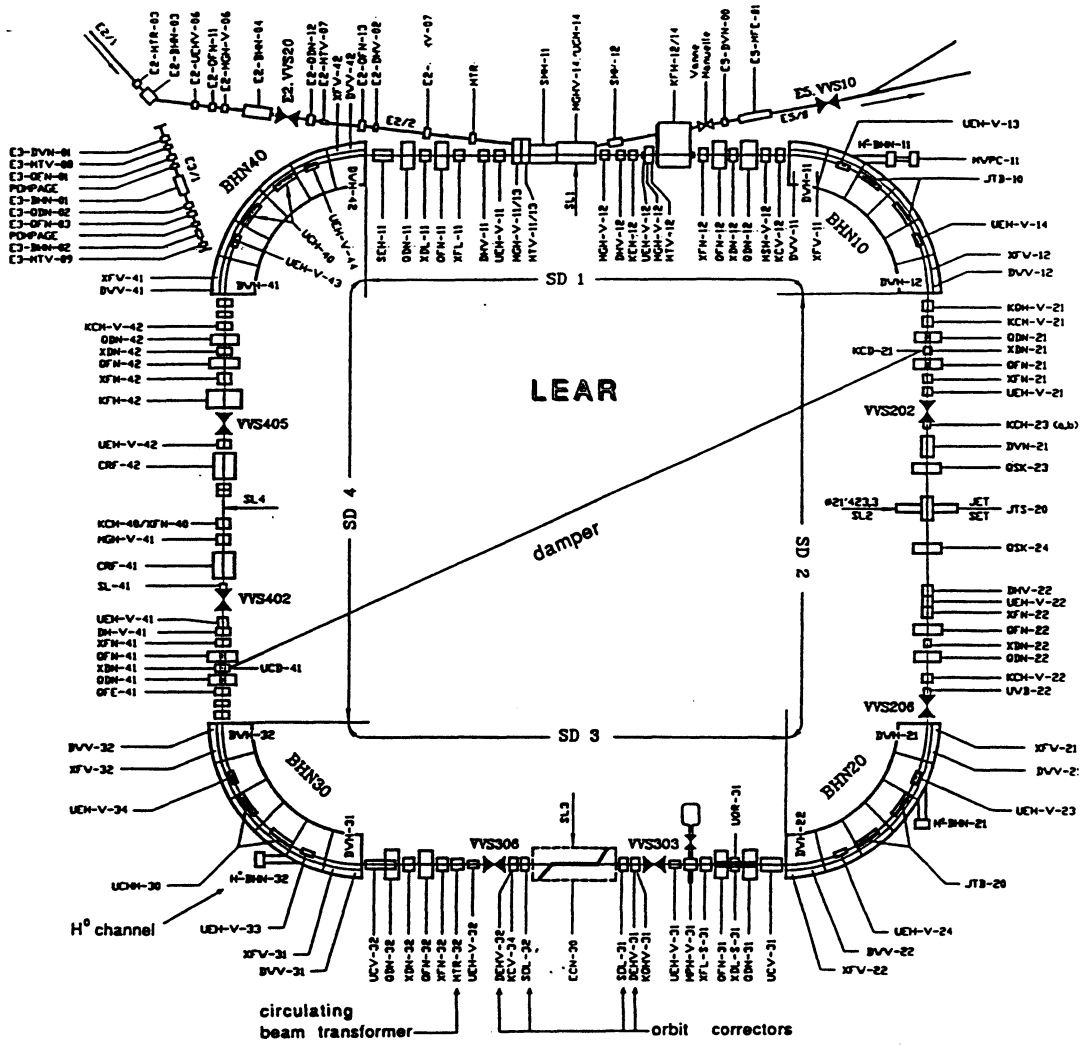

Fig. 1 - The LEAR machine

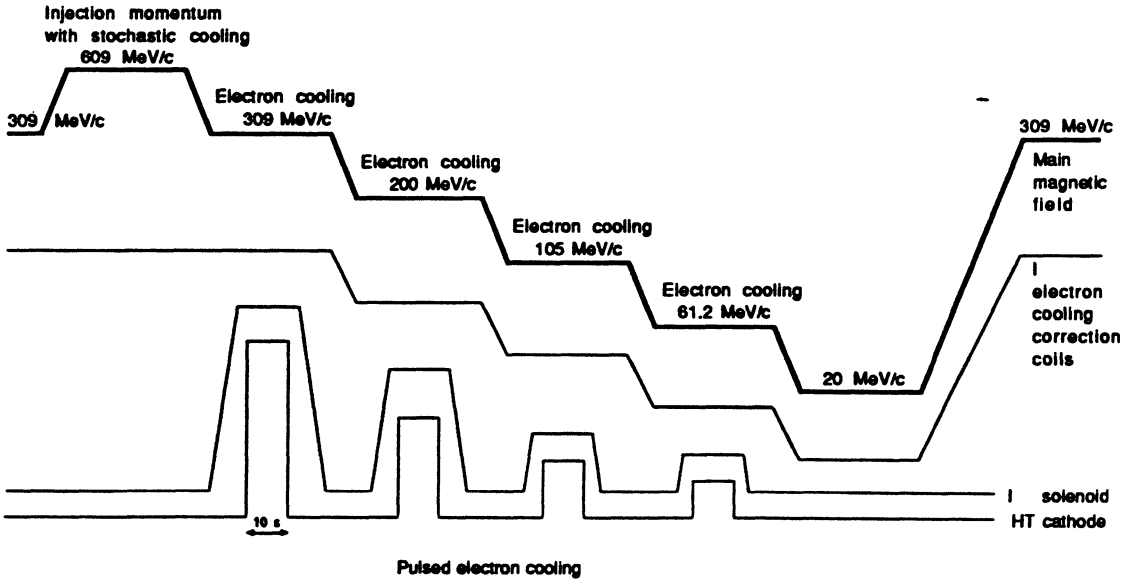

Ultra slow extraction 0.5-3 hrs possible at all momenta , fast extraction also used at 105 and 61.2 MeV/c

Fig. 2 - A typical LEAR cycle

Table 1 - Basic LEAR parameters

Momentum range achieved	0.061–2.0 GeV/c (design 0.1–2.0 GeV/c)
Injection momentum	609 MeV/c
Spill length	0.5–3 hours and fast extraction
Focusing structure	4 super periods, separ. function BoDFOFDoB
Bending magnets: n°, arc length, max. field	4, 6.55 m, B = 1.6 T
Quads: n°, magnetic length, max. gradient	16, 0.5m, k = 1.8 m^{-2} (G = 12 T/m)
Betatron wave number	$Q_h = 2.315$, $Q_v = 2.730$
Vacuum system pressure	10^{-11}–10^{-12} Torr
RF system frequency range (h = 1)	0.4–3.5 MHz (h = 2 below 100 MeV/c)
Aperture limitations	$a_h = \pm 70$ mm, $a_v = \pm 29$ mm

3. THE ELECTRON COOLING DEVICE

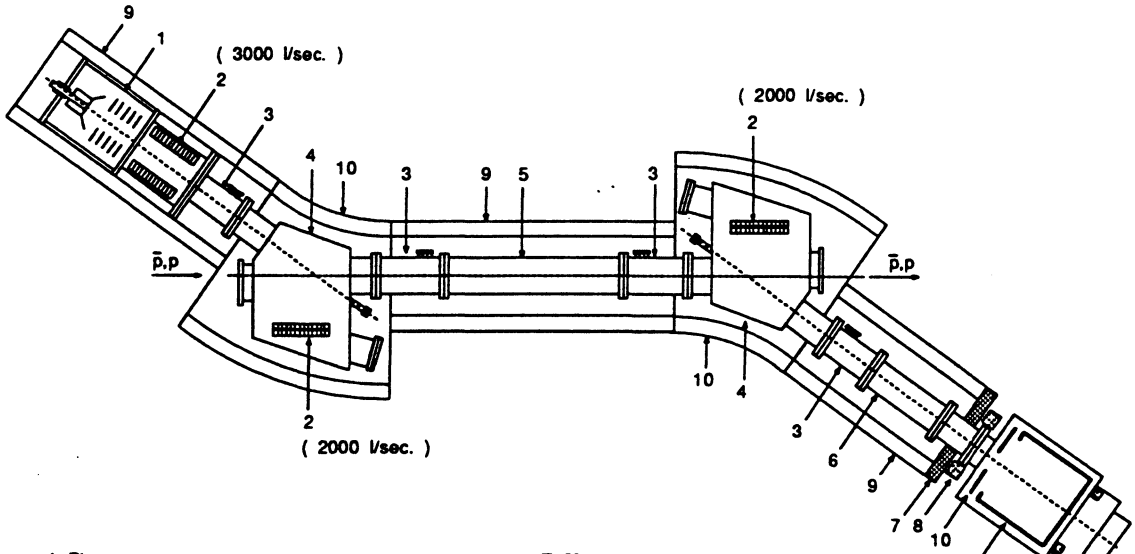

1 Electron gun
2 NEG pumps
3 Pick-up station
4 Toroid chamber with pump and diagnostic ports
5 Central drift tube
6 Collector drift tube
7 Vacuum valve
8 Collector entrance coil
9 Solenoid
10 Repeller
11 Collector
12 Collector end coil

Fig. 3 - The electron cooling device

The LEAR cooler (Fig. 3) is situated at the centre of the third straight section of the LEAR machine (Fig. 1) and has the task of cooling particles with an equivalent momentum up to 309 MeV/c ($\beta = 0.312$). The electron beam is generated in an electron gun where it is accelerated to

the desired energy via four ring shaped anodes. It is transported in a solenoidal field and bent into the cooling section by a 36° toroid magnet. After the cooling section, which is 1.5 m long, the electrons are deflected by another toroid and are recuperated by the collector. The original collector device came from the ICE set-up (Initial Cooling Experiment made at CERN in 1978), but due to reliability problems was replaced by a much simpler design [3]. It consists of a Faraday cup and a repeller electrode at the entrance of the collector which has the role of decelerating the electrons before their collection. A vacuum valve has been installed between the collector solenoid and the collector itself for the purpose of easy maintenance. This 'gap' in the magnetic field is compensated by a coil placed just before the collector entrance. Because of the new collector, electron recuperation efficiency has improved by a factor of 10 and has enabled the cooler to be used routinely for low energy operation.

The operational mode retained for use on the LEAR deceleration cycle is the so-called 'pulsed mode' [4], as described in Fig. 2. The collector and repeller voltages as well as the field of the collector entrance coil are kept fixed throughout the cycle, while the correction coils are ramped following the LEAR magnetic cycle. The accelerating voltages, applied to the cathode and the anode, and the solenoid current are put on for 10 seconds on the standard 'flat-tops' which is ample time for cooling. In this way the solenoid does not perturb the beam during the actual deceleration.

Using this method, the beam characteristics are greatly improved and some 15 minutes can be saved when decelerating a beam to 105 MeV/c as opposed to using stochastic cooling. Typical electron cooling parameters are shown in Table 2.

Table 2 - Typical parameters for electron cooling

Ion beam momentum (MeV/c/n)	116.0	147.0	308.6	200.0	105.0	61.2
Ion type	O^{8+}	O^{6+}	$p/\bar{p}$	$p/\bar{p}$	$p/\bar{p}$	$p/\bar{p}$
Electron beam energy (keV)	4.12	6.22	27.2	11.78	3.27	1.1
Electron beam current (A)	0.305	0.150	2.4	0.640	0.094	0.019
Solenoid field (G)	173.	216.	448.	293.	154.	90.

4. COOLING RESULTS

A number of measurements have been made in order to determine the efficiency of the longitudinal cooling with the different particle types. Transverse emittances have also been measured using scrapers or, when possible, using the neutral hydrogen channel. Finally cooling times in the transverse planes were measured by observing the evolution of the Schottky spectra during the cooling process [5].

4.1 Longitudinal Cooling Times

For this measurement two methods have been tested. The first consists in stepping away the electron-beam energy via the high-voltage power supply and then resetting it to the operational value. One observes the longitudinal spectral density in a narrow bandwidth around a harmonic of the revolution frequency. The spectrum analyser is triggered at the same moment as the high-voltage step. In this way the time it takes for the beam to move back to nominal energy can be measured and the cooling time can be estimated.

The second method is similar to the first but instead of stepping away the voltage, radio-frequency (rf) noise is applied across a longitudinal gap at a harmonic of the revolution frequency. The bandwidth and the power of this noise voltage can be adjusted in order to blow the beam up to a momentum spread of about 1%. When the noise is switched off the spectrum analyser is triggered and the evolution of the spectral density is observed.

Examples of the signals observed are shown in Figs. 4 to 7.

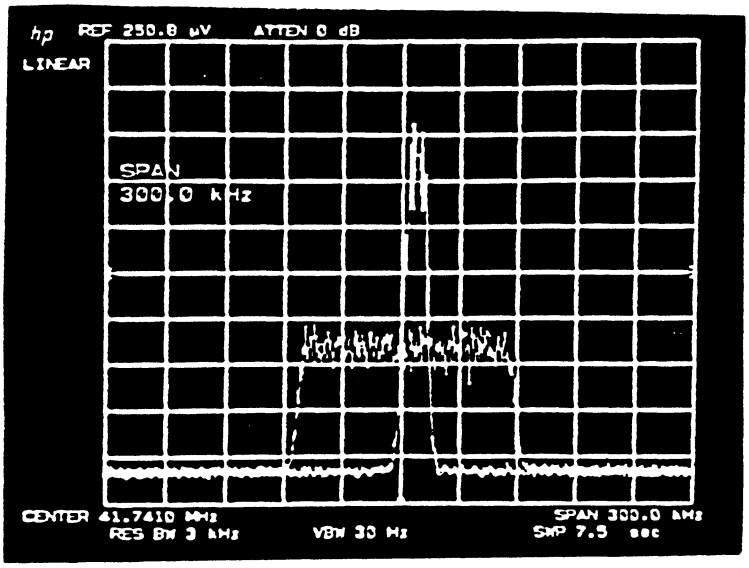

Fig. 4 - Longitudinal beam distribution of a proton beam with and without the heating noise.

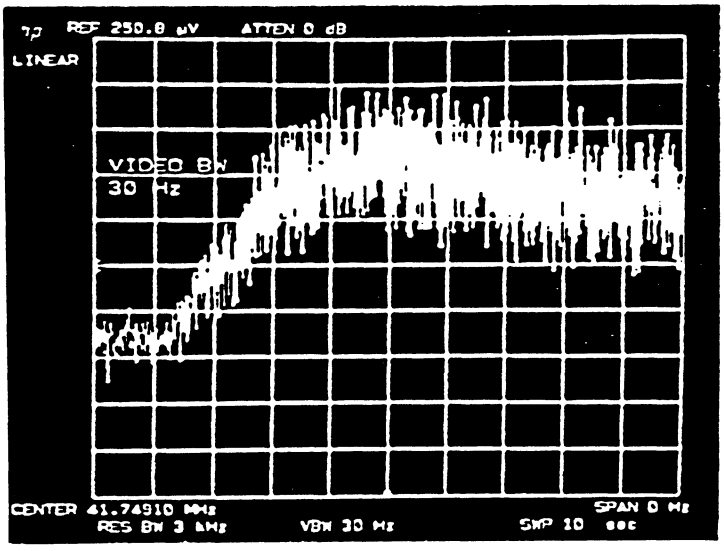

Fig. 5

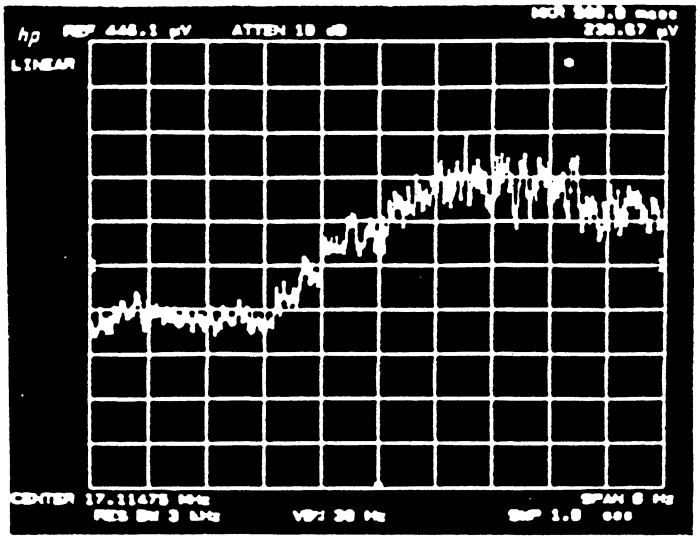

Fig. 6

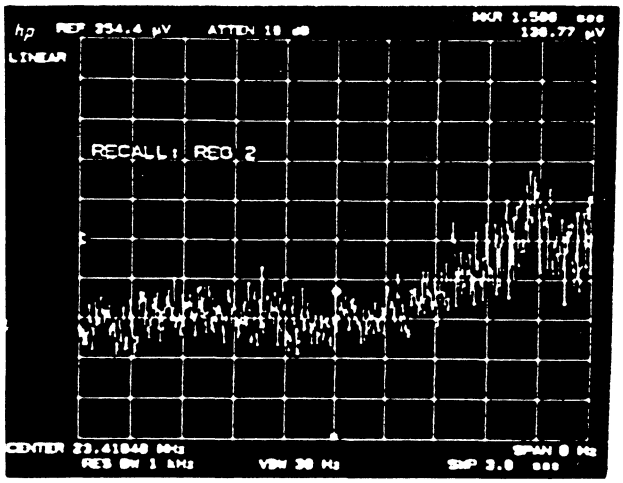

Fig. 7

Figs. 5 to 7 - Longitudinal cooling time measurements for protons, O^{8+} and O^{6+} ions. The curves show the time evolution of the longitudinal Schottky signal (which is proportional to the square root of the particle density as long as the shielding effects (see chapter 6) are negligible. The density increases when the heating noise is switched off. The horizontal scale is 1s/div. in Fig. 5, 0.1 s/div. in Fig. 6 and 0.3 s/div. in Fig. 7.

4.2 Longitudinal frictional force

In order to determine the frictional force (from which the cooling time can be derived) yet another method was developed. It is based on analysing the distribution in equilibrium between a constant heating power and electron cooling at low relative velocities. The measurement was performed in the following way. A rf noise with a bandwidth of 10 kHz and a power of 5 μW/Hz was injected onto a cooled beam at 13.126 MHz on a rf gap. This produces a broader distribution of the momentum spread which can be increased or reduced by varying the attenuation of the noise. To obtain the velocity dependence of the frictional force $F(v)$ from the equilibrium distribution $\rho(v)$, one has to solve the one-dimensional Fokker-Plank equation for a frequency-independent diffusion-constant D :

$$\frac{\partial \rho}{\partial t} = \frac{\partial}{\partial v}\left(-F(v)\rho(v) + D\frac{\partial \rho}{\partial v}\right)$$

In the equilibrium case $\partial\rho/\partial t = 0$, the frictional force is determined by the normalised slope of the distribution function:

$$F(v) = \frac{D(\partial\rho/\partial v)}{\rho(v)}$$

The diffusion constant D is derived experimentally from an independent measurement of the diffusion without the cooling force. Figure 8 shows the result of two measurements made with 50 MeV antiprotons, one with aligned beams and the other with misaligned electron and proton beams (angle of about 1 mrad).

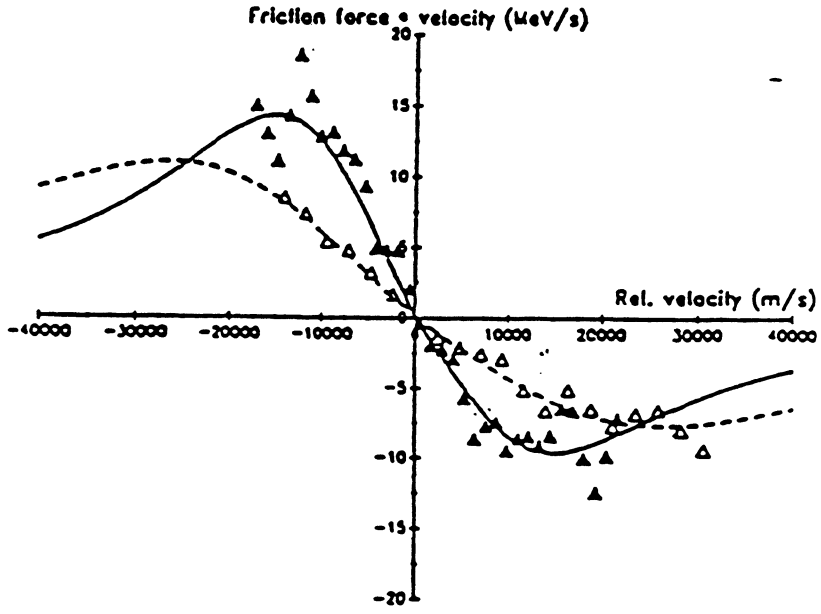

Fig. 8 - The longitudinal frictional force $F(v)$ as a function of v for 50 MeV antiprotons where v is the difference between the ion and the electron velocities. The filled triangles correspond to the measurement made with aligned beams and the unfilled triangles to the measurement with misaligned beams.

4.3 H^-,O^{8+} and O^{6+} ions

The aim of the tests with H^-, O^{6+} and O^{8+} ions was to obtain some idea of the lifetime of different ions in a good vacuum cooler ring and to eventually test the cooling and the stacking of ions [6]. With H^- ions we found that the lifetime was greatly reduced under electron cooling. This is probably due to intra-beam stripping where the loosely bound electron is stripped off in a near collision with another H^- of the same beam forming a neutral hydrogen atom which is lost. The beam-intensity evolution measured on the circulating beam transformer with and without electron cooling is shown in Fig 9. As a consequence precise cooling time measurements were impossible even though the reduction in momentum spread was quite important (Fig. 10).

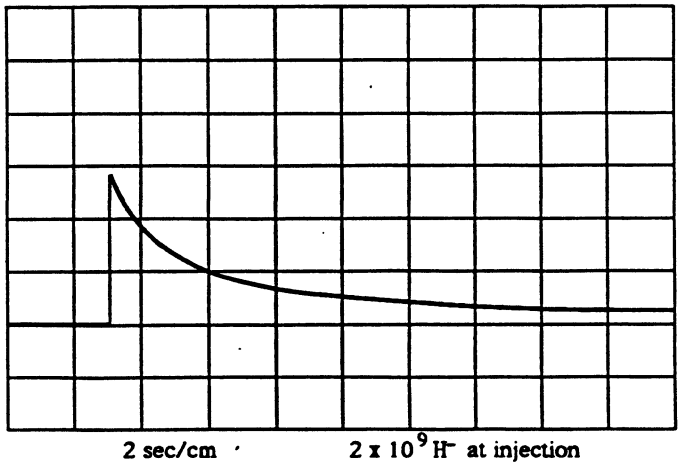

(a)

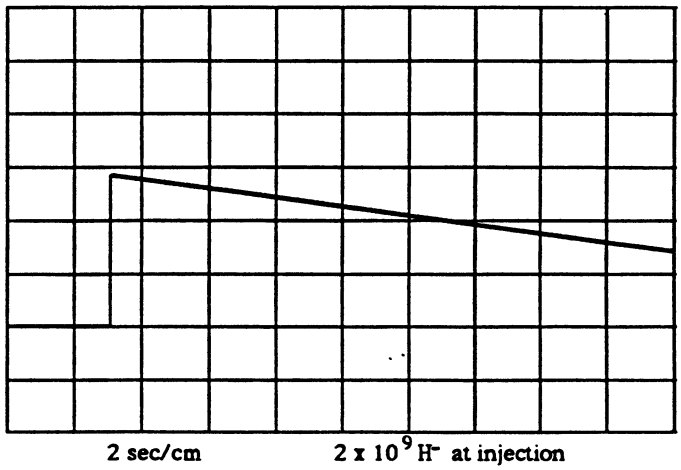

(b)

Fig. 9. Beam-intensity evolution of H^- ions with (a) and without (b) electron cooling

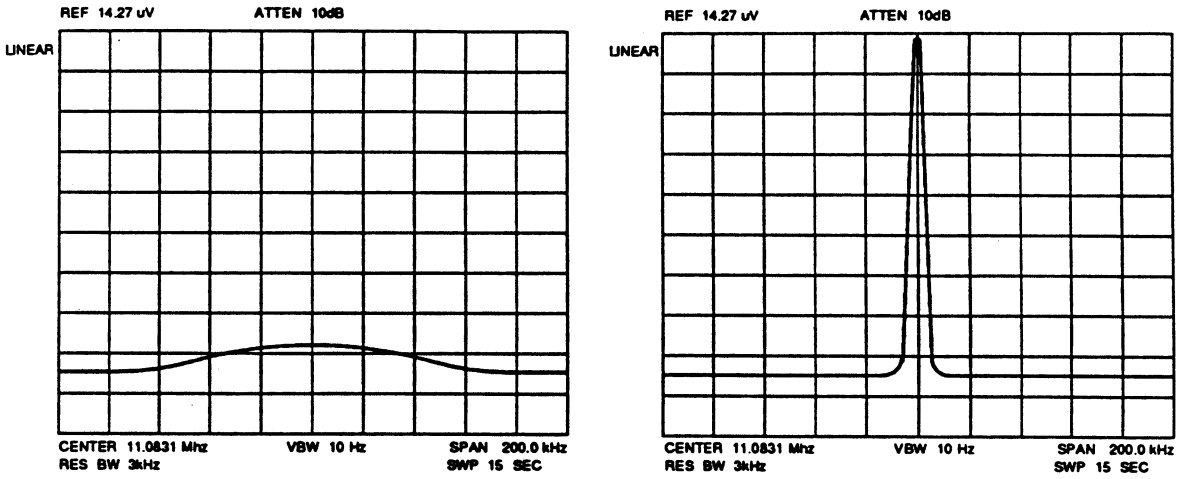

(a) *(b)*

Fig. 10 - Longitudinal Schottky scan of H^- ions just after injection (a) and with electron cooling (b). Horizontal scale: $\Delta p/p = 2 \times 10^{-4}$/div.

With oxygen ions we were able to make a series of measurements on the longitudinal cooling time. The method used was that based on the heating by noise as described in section 4.2. Measurements with different momentum spreads and different intensities were made in order to compare with the results obtained with protons and to check the A/Z_i^2 dependence of the cooling time, where A is the mass number and eZ_i the charge of the ion. The results are summarised in Table 3.

Table 3 - Cooling times measured for different particles as a function of initial momentum spreads and intensities

Initial $\Delta P/P$ (10^{-3})	Final $\Delta P/P$ (10^{-4})	Total cooling time (s)	Particle type	Number of charges (10^9)
3.5	6.0	0.600	O^{8+}	5.8
2.7	6.0	0.500	O^{8+}	5.5
1.8	6.0	0.350	O^{8+}	5.2
5.5	8.0	1.90	O^{6+}	10
1.7	8.0	0.700	O^{6+}	10
3.3	9.0	1.10	O^{6+}	10
2.8	5.0	3.50	p	3
1.9	5.0	2.90	p	3
5.6	5.0	6.60	p	3

From the above table one might conclude that the A/Z_i^2 scaling law for the cooling time does not completely hold. However, it must be mentioned that our measurements do concern the time to reach the final equilibrium and not the e-folding time $\tau \propto \beta^3\gamma^5 A/Z_i^2 n_e$ (where n_e is the electron beam volume density). We must also be careful in our interpretation of the observed signals as many strange phenomena, such as an energy shift during cooling or the onset of the double peak structure, give the impression of a longer cooling time. We should further mention that due to the fact that the initial distribution is rectangular the cooling will naturally be longer than in the case of a Gaussian distribution. Finally the parameters of the electron beam, like its density and its alignment with the ion beam, enter critically into the comparison. These parameters can easily vary from run to run. More work is needed to assess these questions .

4.4 Stacking of ions

Since transverse stacking in LEAR is impossible without major modifications, a longitudinal scheme was tried.

The multi-injection of ions is performed in four consecutive phases. Figure 11 illustrates the principle of this injection mode where the two LEAR rf cavities (CRF41 and CRF42) are working respectively on the first (h = 1) and second (h = 2) harmonic of the revolution frequency. This effectively means that the circumference of the machine can be divided into two halves corresponding to what will be called the "injection bucket" and the "stack bucket". The four phases are outlined as follows:

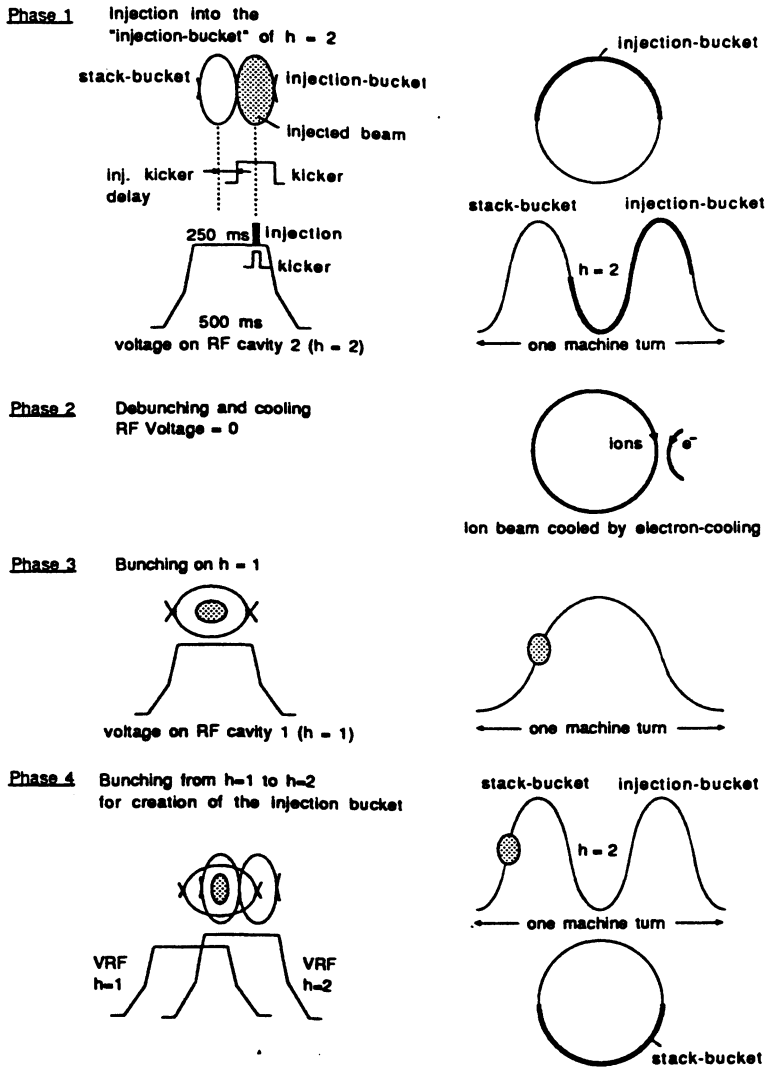

Fig. 11 - Principle of the multi-injection process using two rf cavities

1. The stack is concentrated in one of the $h = 2$ buckets (the stack bucket). The injection kicker is triggered, synchronised on the rf cavity and delayed in such a manner that the injected beam will fall into the injection bucket.
2. A few milliseconds after injection the rf voltage is reduced to zero and the beam is debunched filling the whole circumference of the machine. Electron cooling, which is on during the whole process, reduces the momentum spread and the transverse emittances of the coasting beam for another 1.8 s.
3. CRF41 is then set on and bunches the beam on $h = 1$.
4. CRF42 is brought to its nominal voltage with the right phase so that the cooled bunched beam is trapped within the "stack bucket" and the empty "injection bucket" is filled as in point 1.

Using this method up to 14×10^9 charges of O^{8+} ions could be accumulated, the limit being due to losses in the rf gymnastics. It was therefore decided to inject using only one rf cavity working on $h = 1$, with a voltage high enough to contract the stack into a short bunch at the stable phase and to inject a new batch on the unstable phase. The voltage is immediately

reduced after injection, the newly injected particles are rapidly cooled by electron cooling and the injection process can start again. The principle of the injection scheme is shown in Fig. 12. In this manner we managed to rapidly accumulate 64×10^9 charges of O^{8+} ions and 46×10^9 charges of O^{6+} ions [7] from linac pulses of $2\text{-}5 \times 10^8$ charges .

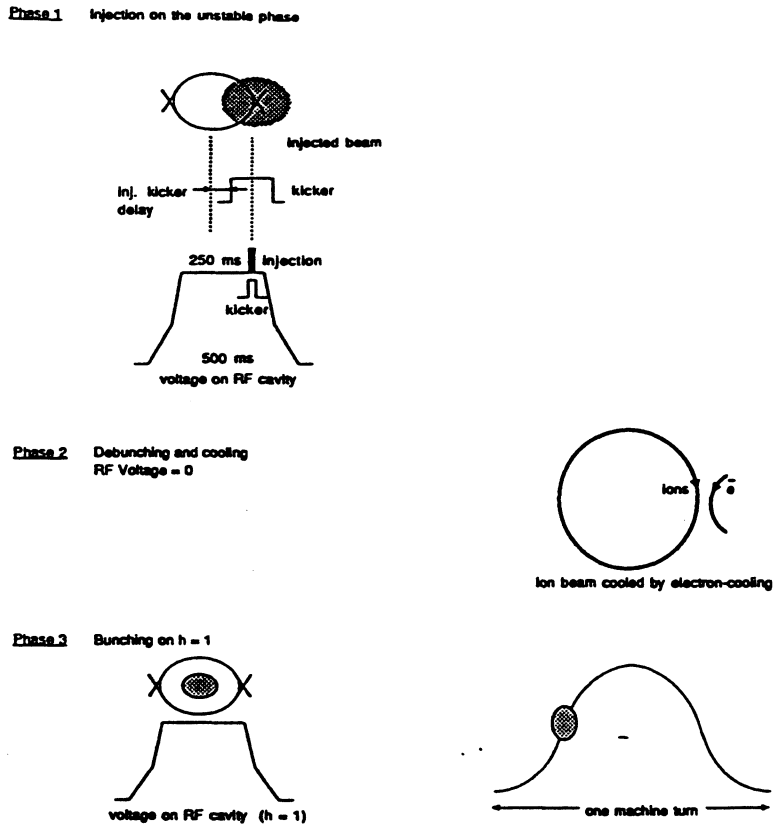

Fig. 12 - Multi-injection process principle with just one rf cavity

Due to imperfections of the set-up about 1% of the stack was lost during each injection. This explains the saturation at a stacking factor of ≅100. For O^{6+} additional losses due to charge exchange with the residual gas (leading to a beam half life of about 200 s) introduced the further reduction of the stacking efficiency.

5. INSTABILITIES

5.1 Observation of Instabilities

Transverse instabilities can be observed on both large bandwidth Schottky pickups, and at low frequency with the position pickups. If a spectrum analyser is used to observe the variation in amplitude of an $(n\text{-}q)$ sideband as a function of time, the instability manifests itself by an abrupt rise in the amplitude. This is followed by a cooling period of about 1 to 10 seconds (depending on the emittance of the beam after the instability) before the threshold is reached again. In the simple case of a dipole type instability where the beam oscillates like a string, the beam centre is represented by a travelling wave type of oscillation with an amplitude $x(t)$ which grows exponentially in time:

$$x(s,t) = x_0 e^{i[(n\pm q)\omega_r t \pm (ns/R)]}$$

Here n is the mode of the oscillation and q the non-integer part of the betatron tune $Q(Q=|Q|+q)$ At fixed azimuth a pickup will see the mode frequency $\omega_n = (n \pm Q)\omega_r$. We found that the low-order, $n \leq 3$, slow waves (i.e. the n-q bands as opposed to the n+q "fast waves") were the most unstable at LEAR. Figures 13 and 14 show the typical signals observed when the beam is unstable.

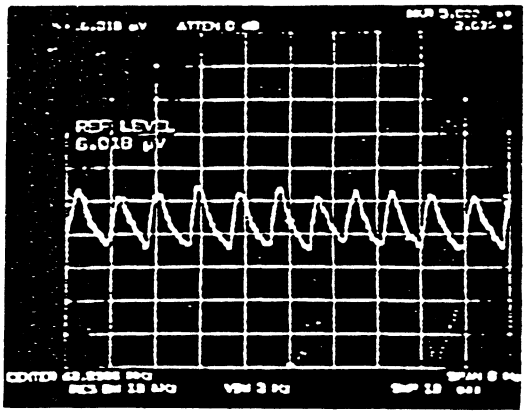

Fig. 13 - Transverse instabilities observed on a Schottky pickup. Time evolution of the density. The height of the signal, near 40 MHz, is displayed and the instability (occurring at lower frequencies) causes a large coherent oscillation which smears out and leads to an emittance growth. This growth leads to the jumping up of the signal .This blow-up is then compensated by the cooling before the next burst of instabilities occurs. Horizontal scale 1 sec/div.

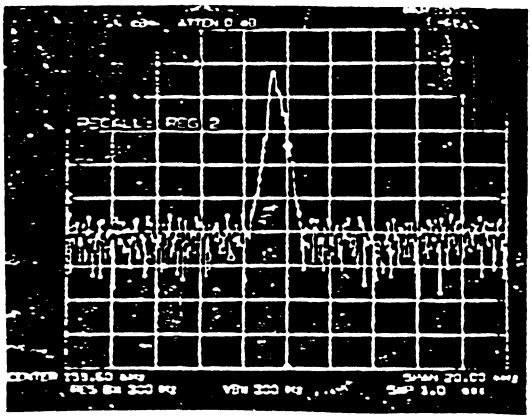

Fig. 14 - Transverse instabilities observed on a position pickup. The figure displays the spectral density at low frequency near the 1-q band. This is one of the bands where the instability occurs. The spike representing the beam oscillation jumps up with each burst of the instability.

5.2 The Causes of Instabilities

During the cooling process the beam density $N/\varepsilon_h \varepsilon_v \varepsilon_l$ increases and once it reaches a given threshold the ion beam will become unstable and perform coherent betatron oscillations. Under normal circumstances a beam will resist coherent instabilities by virtue of Landau damping. A small difference in the oscillation frequency prevents the ensemble to respond coherently to the driving force exerted on it by beam induced fields. However, cooled beams are susceptible to respond coherently for two reasons:

1) the tune spread due to non-linearities and the momentum spread decreases,

2) the induced fields, such as direct space-charge transverse fields, increase as the beam is cooled down.

From the mode frequency we can define a mode frequency shift $\Delta\omega_n = \pm\Delta Q\omega_r$, which is due to beam induced fields, and a mode frequency spread $\delta\omega_n = (n\pm Q)\delta\omega_r \pm \omega_r\delta Q$, which is due to tune and revolution frequency spreads. If the mode frequency shift has an imaginary part, the oscillation can self amplify. As a rule of thumb we can say that the stabilisation of transverse instabilities by Landau damping requires that:

$$|\Delta\omega_n| \le (1/\pi)|(n\pm Q)\delta\omega_r \pm \omega_r\delta Q|$$

For the longitudinal plane the "Keil-Schnell criterion" states that the momentum spread should be large enough to ensure stability namely, as a rule of thumb, the required momentum spread is given by:

$$\left(\frac{\Delta P}{P_0}\right)^2_{FWHM} \ge \left|\frac{Z_\parallel}{n}\right| \frac{Z_i e}{m_i c^2} \frac{I_i}{\beta_0^2 \gamma_0 |\eta|},$$

where

$Z_i e$ is the ion charge,

$I_i = NZ_i e f_0$ is the ion-beam current,

$m_i = Am_p$ is the ion mass and

$Z_\parallel$ is the longitudinal coupling impedance seen by the beam at nf_r ,

$\eta = (1/\gamma^2)-(1/\gamma_{tr}^2)$ is the off-momentum factor of the storage ring.

The contribution of space-charge forces to the coupling impedance is about:

$$\frac{Z_\parallel}{n} = \frac{-i\,377\,g}{2\beta_0\gamma_0^2} \text{ ohm}$$

where the geometrical factor g is expressed by:

$$g = 1 + 2\ell n\left(\frac{\text{chamber half - height}}{\text{beam half - height}}\right) = 1 + 2\ell n\left(\frac{b}{a}\right)$$

From these formulae one can see that the space-charge contribution dominates at low energies .

The above-mentioned criterion for the transverse stability can also be expressed in terms of a "transverse impedance" $Z_\perp$. Taking only the momentum-dependent spreads into account we can write :

$$Z_\perp \le \pi F \frac{m_i c^2}{Z_i e} \frac{\beta^3\gamma}{(R/Q)I_i} \frac{\Delta p}{p} |(n\pm Q)\eta \pm \zeta Q|$$

where

F = a form factor of the order of 1,

R = the mean radius of the accelerator,

Q = the tune and

ζ = the chromaticity ($\zeta = (\partial Q/Q)/(\partial p/p)$);

$Z_\perp$ is the transverse impedance, at the mode frequency $(n\text{-}Q)f_r$, related to the longitudinal impedance via $Z_\parallel/n = (b^2/R)(Z_\perp/|n\text{-}Q|)$. This is valid for simple structures but not for the space-charge contribution to the transverse impedance, whose imaginary part for a coasting beam is about:

$$\frac{Z_\perp}{|n-Q|} = \frac{377R}{\beta_0^2\gamma_0^2}\left(\frac{1}{a^2}-\frac{1}{b^2}\right) \text{ Ohm / meter}$$

We can thus see how the electron cooling may contribute to the transverse instability since during the cooling process a and Δp are drastically reduced.

Other contributions to the impedance come from the wall resistivities, the vacuum-chamber size changes, rf cavities, ferrites and dielectric structures seen by the beam. Hence the importance of actually measuring the impedance. Section 6 is devoted to this subject.

5.3 Feedback Systems.

The feedback system (or 'damper') developed to counteract these coherent transverse instabilities consists of a pickup system used for the detection of the instability and a kicker system placed at an odd number of quarter wavelengths of the betatron oscillation away from the pickup (Fig. 15, and Ref [8]). The signal observed at the pickup is passed through a de-skew buffer which generates a horizontal and a vertical position signal. These are then linearly amplified, delayed and then put through a skew hybrid before being applied to the kicker plates (Fig. 16). The bandwidth of the system is determined by the number of modes to be corrected and the gain by the growth rate of the instability. In our case a band from 70 kHz to 70 MHz is desirable to cover the first 20 modes in the whole energy range of LEAR. To maintain damping during energy damping, a closed orbit suppresser (COS) has also been developed as this is needed for suppressing the strong coherent signal observed when a bunched beam is not properly centred in a position pickup.

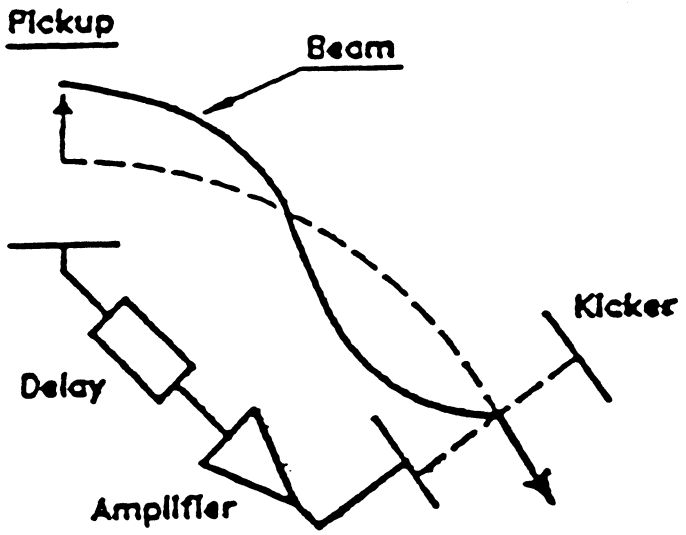

Fig. 15 - Principle of the transverse feedback system

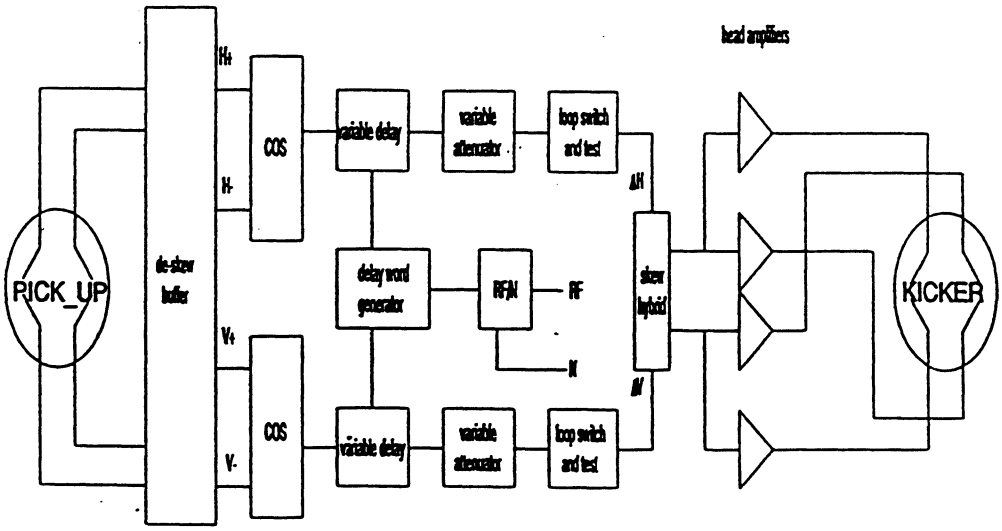

Fig. 16 - LEAR damper block diagram

6. IMPEDANCE MEASUREMENTS.

In order to perform impedance measurements the ion beam is excited , through a kicker, by an electrical noise of a given bandwidth, and the response to this excitation is measured by a pickup (Fig. 17). The ratio r = response/excitation is evaluated using a Fast Fourier Transform (FFT) analyser. We have to distinguish the ratio, named r^0, ignoring the coupling of the beam with its surroundings from the measured ratio, r^c, influenced by the coupling. In analogy with a feedback system we can introduce an impedance Z to describe the coupling effect ($Z_{\parallel}$ for the longitudinal coupling and $Z_{\perp}$ for the transverse coupling).

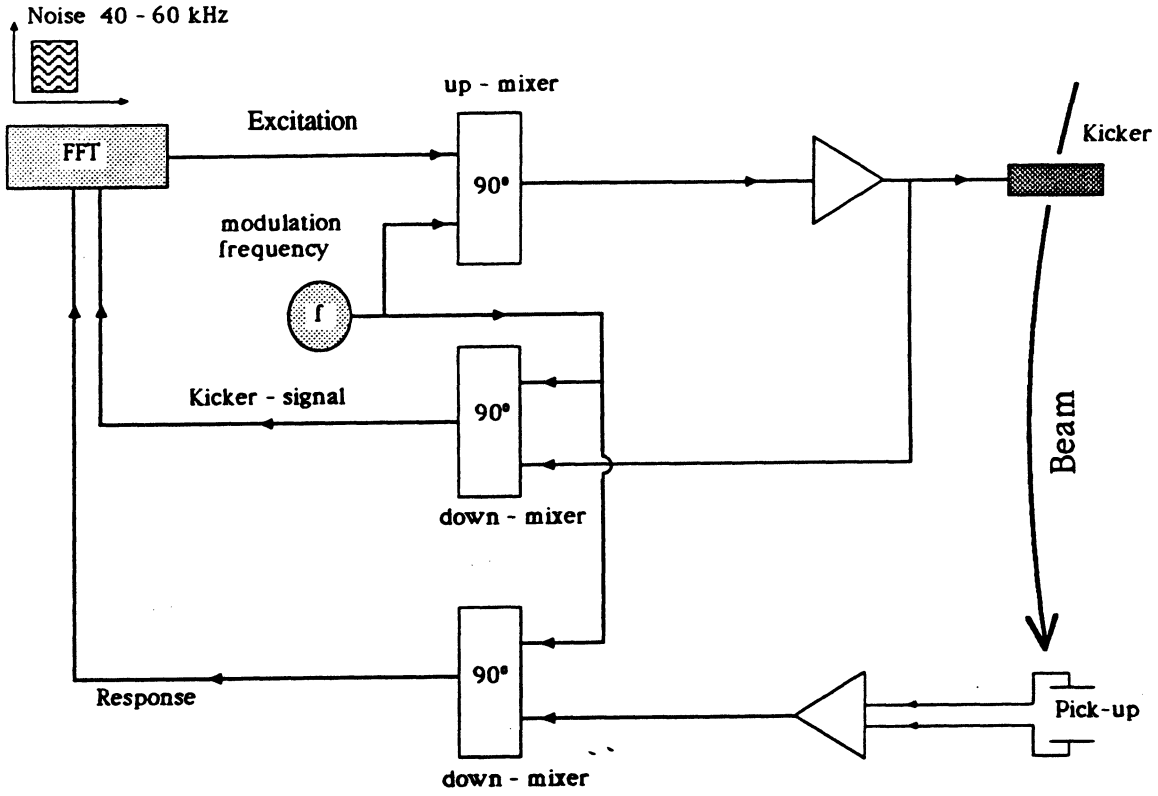

Fig. 17 - Impedance measurement set-up

It is well known [9] that the response r^0 of a circulating beam to a sinusoidal excitation is proportional to the dispersion integral $D(\omega)$. In the longitudinal plane it is given by:

$$D(\omega) = \int \frac{(\partial\psi/\partial\omega_r)}{(\omega - n\omega_r)} d\omega_r = PV \int \frac{(\partial\psi/\partial\omega_r)}{(\omega - n\omega_r)} d\omega_r + i\frac{\pi\partial\psi(\omega_r)}{n\partial\omega_r}\Big|_{\omega_r=(\omega/n)}$$

with :

ω = the excitation frequency,
$\psi(\omega_r$ = the revolution frequency distribution, normalised such that $\int\psi d\omega_r = 1$,
ω_r = the particle revolution frequency, with the average $\omega_0 = 2\pi f_0$,
PV = the principal value of the integral and
n = the harmonic number.

Taking r^0 as:

$$r^0 = iI_i \frac{\eta}{\gamma_0\beta_0^2} \frac{Z_i e}{m_i c^2} \omega_0^2 D(\omega)$$

the beam transfer function (BTF) r^c, in the presence of a longitudinal coupling impedance $Z_\parallel$ is then related to response r^0 by

$$r^c(\omega) = \frac{r^0(\omega)}{1 + Z_\parallel r^0(\omega)} = \frac{r^0(\omega)}{\varepsilon_\parallel},$$

where $\varepsilon_\parallel$ is the so-called "dielectric function" or "shielding factor". One sees that the above response tends to infinity when $Z_\parallel r^0(\omega) = -1$. This indicates that depending on the value of $Z_\parallel$ the beam can become unstable. The limiting value for the impedance corresponds exactly to the threshold conditions discussed in section 5.2 above. Figure 18 shows a plot of a computer simulated BTF. This inverted response diagram in the complex plane or more precisely:

$$\frac{1}{r^c(\omega)} = \frac{1}{r^0(\omega)} + Z_\parallel$$

is shifted by $Z_\parallel$ and the beam is close to an instability threshold ($r^c \rightarrow \infty$)when the curve touches the origin. The determination of the impedance, and of the stability limits by analysis of the BTF diagram is therefore of great interest [10]. The inverted response is also called "stability diagram".

At LEAR, BTF measurements have been carried out with protons, O^{8+}, and O^{6+} ions. Figure 19 shows the "stability diagram" $1/r^c$ calculated from a BTF measurement with an O^{8+} beam. From the response r^0, deduced from r^c by shifting the stability curve towards the origin by the expected impedance vector, the true frequency distribution of the beam can be obtained. The frequency distribution can also be obtained through the Schottky power spectrum $P^c(\omega)$ which is modified by the square of the shielding factor ε.

$$\psi(\omega/n) \propto |\varepsilon|^2 P^c(\omega)$$

A criterion for the exactness of the estimated $Z_\parallel$ is that the distributions obtained by the two computations do fit (Fig. 20).

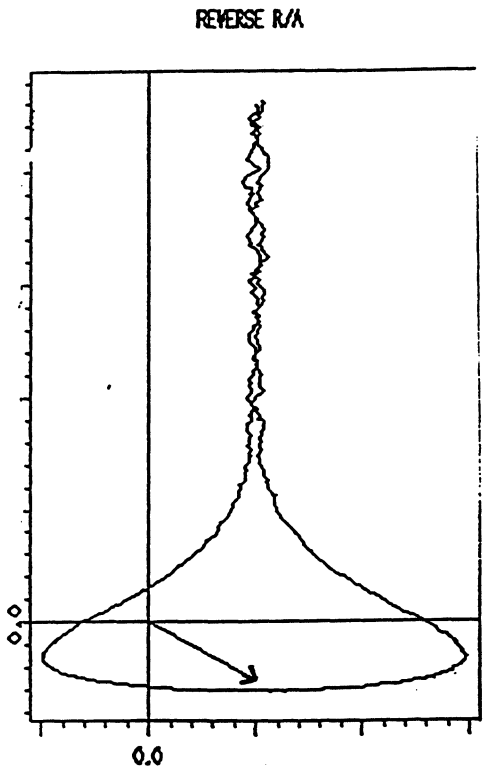

Fig. 18. Computer simulated BTF. $Re\{Z/n\} = -0.2Im\{Z/n\}, f_{rev} = 800$ kHz, $\Delta P/P = 3 \times 10^{-4}$

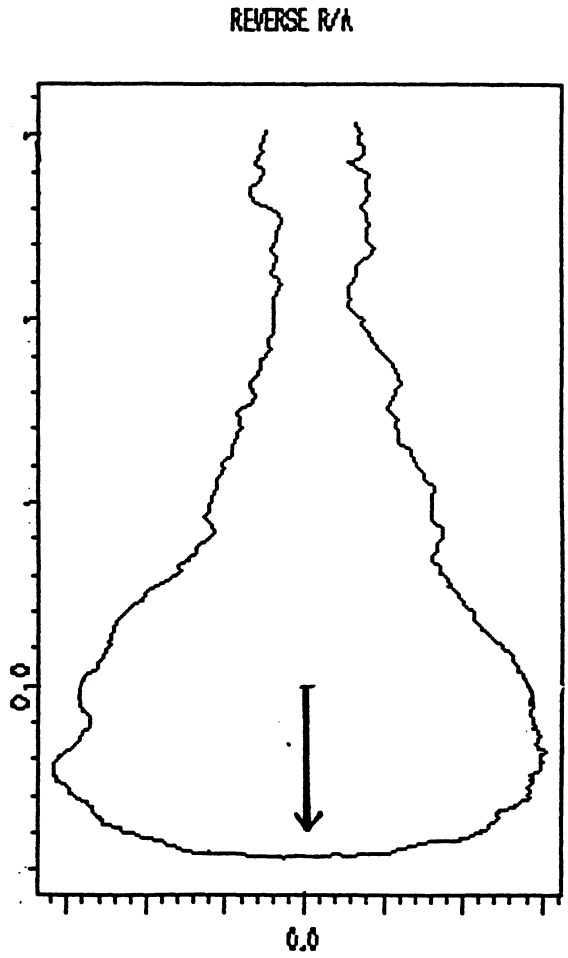

Fig. 19. Measured stability diagram for 5.8×10^{10} O^{8+} charges. The curve is shifted along the imaginary axis by the arrow because the impedance is mainly capacitive

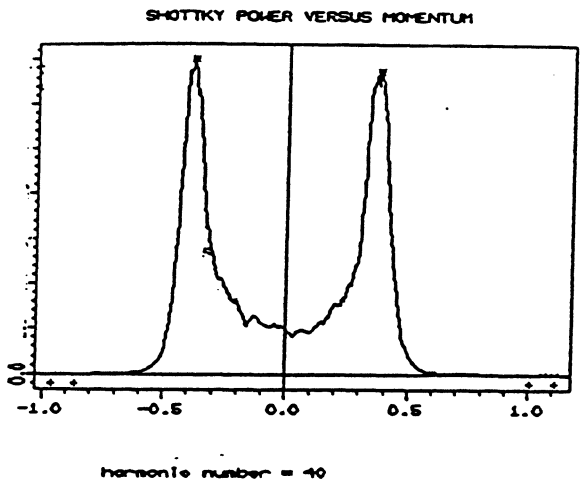

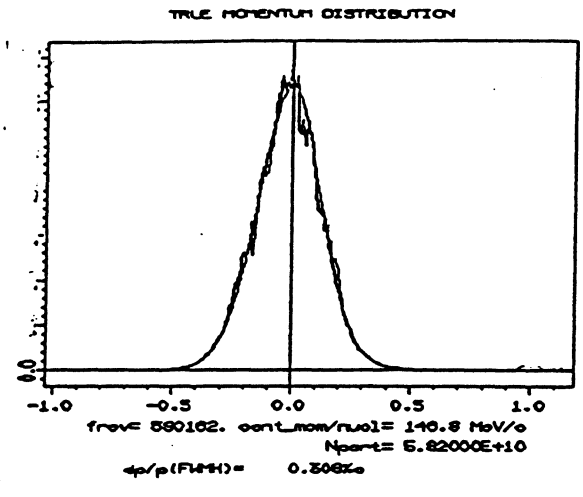

Fig. 20. Reconstructed momentum distribution for the beam of Fig. 19. The picture on the left shows the Schottky power distribution ,including the shielding factor, and on the right the true momentum distributions obtained from the Schottky scan and from the BTF. The estimated impedance vector is: $Re\{Z/n\} = 30\Omega, Im\{Z/n\} = -4.5$ kΩ.

Measurements made at different harmonics have shown a constant value of the imaginary part of the impedance (Fig. 21),which roughly agrees with the space-charge contribution.

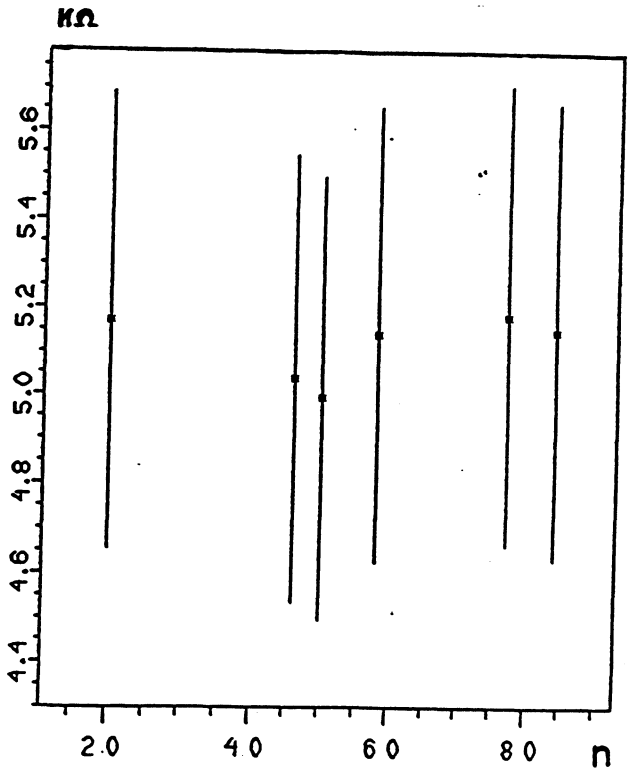

Fig. 21 - $Im\{Z/n\}$ at different harmonics of the revolution frequency

For the transverse plane the dispersion integral is given by:

$$D(\omega) = \pm\frac{1}{2Q\omega_0}\int\frac{\psi(\omega_\beta)}{\omega_\beta-\omega}d\omega_\beta = \pm\frac{1}{2Q\omega_0}\left[PV\int\frac{\psi(\omega_\beta)}{\omega_\beta-\omega}d\omega_\beta - i\pi\psi(\omega_\beta)\Big|_{\omega_\beta=\omega}\right]$$

with:

ω_0 = the nominal revolution frequency,
$\omega_\beta = (n\pm Q)\omega_r$ = the mode frequency.

The residue of this integral is proportional to $\psi(\omega)$ and not to its derivative as it is the case for the longitudinal integral. A calculation of the impedance and the momentum distribution has to include the impedance contribution due to the electron cooler and the feedback system. The transverse stability diagram can therefore be used to check the efficiency of the transverse feedback system. In Fig. 22 one can see the stabilising effect of the damper which shifts the response curve away from the origin as the gain is increased .

More work is necessary at LEAR [11] in order to get a better signal to noise ratio in the measurement and the addition of filters in the set-up (Fig. 17) will hopefully lead to an improvement of the measurement accuracy by suppressing the noise coming from higher harmonics.

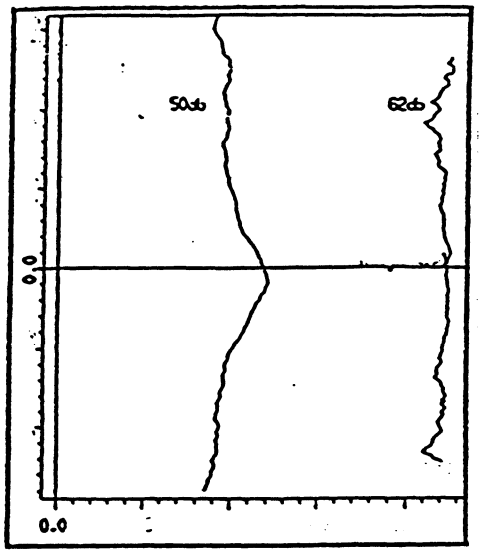

Fig. 22 - Influence of the damper on the stability diagram. The shift of the curve to the right indicates the stabilising effect.

7. FUTURES PLANS

For the future we are developing, in collaboration with INP Novosibirsk and CAPT Lipetsk, a new variable intensity gun [12] which would significantly reduce the cooling time of heavy ions. The gun uses two electrodes, one to determine the electron current and a second to fix the final energy, in an adiabatic optics scheme. This means that its operation is greatly simplified as there are only two electrodes to control and the magnetic field is fixed. Moreover, the electron-beam intensity can be varied in order to always be in a regime where the cooler is most efficient.

In conjunction with the project for the new gun, we hope to install a system for controlled neutralisation of the electron beam. This would facilitate the efficiency of the gun when it works on-line in the variable intensity mode.

8. ACKNOWLEDGEMENTS

We would like to thank all members of the LEAR team for their help. Special thanks to M. LeGras, R. Maccaferri, F. Ollenhauer, J.C. Perrier, T. Pettersson, L. Søby, D.J. Williams and our colleagues from CAPT Lipetsk who helped make the routine use of electron cooling at LEAR a reality. The damper was developed by F. Pedersen and D.J. Williams. Last but not least we are grateful to S. Maury for his continuous encouragement.

9. REFERENCES

[1] a) Bosser J., Chanel M., Ley R., Möhl D., Perrier J.C., Tranquille G., Williams D.J., "Operational Aspects of Electron Cooling at the Low Energy Antiproton Ring (LEAR)", Proc. IEEE PAC'91, San Francisco, USA, pp. 2832-2834.
b) Lefèvre P., "LEAR Present Status, Future and Developments", Proc. of the IVth LEAR Workshop, Villars-sur-Ollon 1987, Harwood Acad. Publishers, 1988, pp. 19-29.

[2] Asseo E., Baird S., Bosser J., Chanel M., Lefèvre P., Ley R., Maccaferri R., Manglunki D., Möhl D., Molinari G., Perrier J.C., Pettersson T., Tranquille G., Vandeplassche D., Williams D.J., "Performance Update of LEAR", Proc. EPAC'92, Berlin, Germany (to be published).

[3] Bosser J., Ley R., Tranquille G., Bykovsky V., Funtikov F., Meshkov I., Polyakov V., Seleznev I., Sinizky V., "The New Collector for the Electron Cooling Device at LEAR", NIM A311 (1992), pp. 465-471.

[4] Bosser J., Chanel M., Ley R., Tranquille G., "Variable Energy Electron Cooling at LEAR", Proc. EPAC'92, Berlin, Germany (to be published).

[5] Bosser J., Chanel M., Ley R., Möhl D., Ollenhauer F., Tranquille G., "Status of Electron Cooling Experiments at LEAR", Workshop on Electron Cooling and New Cooling Techniques, Legnaro, Italy, 1990, eds. R. Calabrese and L. Tecchio (World Scientific 1990), pp. 1-20.

[6] Baird S., Bosser J., Chanel M., Fernandez C., Hill C.E., Lefèvre P., Ley R., Manglunki D., Möhl D., Molinari G., Perrier J.C., Pettersson T., Têtu P., Tranquille G., Williams D.J., "Oxygen Ions in LEAR", Proc. EPAC'90, Nice, France, pp 580-582.

[7] Summary of the 1992 Oxygen ion MD, (to be published).

[8] Lambertson G., "Feedback to Suppress Beam Instabilities in future Proton Rings", Proc. PAC'85, IEEE Trans., NS-32, p. 1857, 1985 .

[9] a) Hübner K., Vaccaro V.G., "Dispersion Relations and Stability of Coasting Particle Beams", CERN-ISR-TH/70-44, 1970.
b) Möhl D., Sessler A.M. "The Use of RF-knockout for the Determination of the Characteristics of the Transverse Instability of an Intense Beam", Proc. 8th Int. Conf. on High-Energy Accelerators, CERN, Geneva 1971, p. 33

[10] Bosser J., Chanel M., Gurevitch M., Manglunki D., Möhl D., Pedersen F., Tranquille G., Vandeplassche D., "Impedance Measurements with Strongly Cooled Beams at LEAR", Proc. IEEE PAC'91, San Francisco, USA. pp. 2509-2511.

[11] Oeftiger U., "Measurement of Beam Properties and Beam Environment in LEAR and COSY Using RF Excitation Methods", Thesis to be published.

[12] Bosser J., Tranquille G., Meshkov I., Poljakov V., Seleznev I., Syresin E., Smirnov A., Zapunjaka A., "Project for a new Variable Current Electron Gun or the LEAR Ecooler", CERN/PS 92-03(AR), 1992.